

## Numerical Analysis on Impact of Crosswinds on the Aerodynamic Performance of Small City Vehicles

Mohammad Arafat<sup>1</sup>, Izuan Amin Ishak<sup>1,\*</sup>, Tiong Woei Ting<sup>1</sup>, Nur Rasyidah Roziman<sup>1</sup>, Nur Amiza Mohd Hairul<sup>1</sup>, Muhammad Aslam Ramli<sup>1</sup>, Zainal Mukhriz Ahmad Puaat<sup>1</sup>, Shahrizal Hafiz Shahmuddin<sup>1</sup>, Ruhendran S. Mahendran<sup>1</sup>, Muhammad Aidil Safwan Abdul Aziz<sup>1</sup>, Andrew Soh Wee Shong<sup>1,2</sup>

<sup>1</sup> Faculty of Engineering Technology, Universiti Tun Hussein Onn Malaysia, Pagoh Campus, 84600, Muar, Johor, Malaysia

<sup>2</sup> School of Industrial Engineering, Telkom University, Bandung, Indonesia

### ARTICLE INFO

#### Article history:

Received 29 November 2024

Received in revised form 1 January 2025

Accepted 7 February 2025

Available online 20 March 2025

#### Keywords:

Aerodynamic; computational fluid dynamics; crosswinds; Reynolds-Averaged Navier-Stokes (RANS); small city vehicles

### ABSTRACT

Small city vehicles are particularly vulnerable to crosswinds due to their lightweight design and higher center of gravity, which reduce stability. Additionally, their aerodynamic shapes can generate lift, making them more susceptible to being pushed off course in windy conditions. This study investigates the aerodynamics of small city vehicles using Computational Fluid Dynamics (CFD) with the Reynolds-Averaged Navier-Stokes (RANS) approach in ANSYS Fluent. The focus is on analyzing the aerodynamic performance of a small city vehicle at a constant speed while subjected to four different crosswind angles: 15°, 30°, 45°, and 60°. A mesh refinement study is conducted to validate the simulations, comparing results from three different mesh configurations to ensure accuracy and reliability. The results indicate that the side force coefficient increases from 1.5 to 5 as the crosswind angle reaches 60°. Additionally, the drag coefficient is observed to be highest at the 30° crosswind angle and decreases to its minimum at the highest crosswind angle. Flow structures show significant complexity at higher crosswind angles. These findings highlight the intricate interactions between the vehicle and crosswinds, providing valuable insights for optimizing the aerodynamic design of small city vehicles to enhance their stability and performance in urban environments.

## 1. Introduction

The aerodynamic design of a vehicle significantly affects its interaction with air, influencing key factors such as drag, stability, and fuel efficiency. In urban environments, where small vehicles are increasingly preferred for their compactness and agility, optimizing aerodynamic performance is essential for improving energy efficiency and enhancing driving safety. Small city vehicles face diverse aerodynamic challenges that necessitate careful design considerations to minimize drag and improve overall performance. For example, the aerodynamic development of vehicles such as the Ford Kuga

\* Corresponding author.

E-mail address: [izuan@uthm.edu.my](mailto:izuan@uthm.edu.my)

<https://doi.org/10.37934/javs.16.1.1022>

highlights the specific challenges faced by smaller vehicles [1]. These challenges are especially important in electric vehicles, which have unique architectural and operational demands that require specialized aerodynamic optimization.

The influence of aerodynamics on vehicle stability and safety is a critical consideration in vehicle design. Poor aerodynamic configurations can lead to increased lift at high speeds, potentially causing instability and reducing traction, which is essential for safe handling on the road. Wu and Wen [2] emphasize that aerodynamic lift can counteract the vehicle's weight, thereby reducing tire-road adhesion, a crucial factor for maintaining control and stability. Additionally, Nath *et al.*, [3] observe that aerodynamic drag is a significant contributor to a vehicle's energy consumption, accounting for approximately 50% of the power required at highway speeds. The growing popularity of small city vehicles is driven by several factors, including increasing traffic congestion and environmental concerns, further underscoring the importance of optimizing their aerodynamic performance.

Crosswinds or lateral winds that affect vehicle stability can significantly influence vehicle performance, particularly at high speeds or on open roads. The interaction between a vehicle and crosswinds generates aerodynamic forces that may lead to loss of control, especially for smaller vehicles. The aerodynamic response of a vehicle to crosswinds is characterized by various forces and moments, including side forces, yaw moments, and rolling moments, which can vary nonlinearly depending on the vehicle's speed and the intensity of the wind [4-6].

Small city vehicles, due to their lighter weight and compact size, face unique challenges under crosswind conditions. These vehicles typically have a higher center of gravity and a smaller aerodynamic profile compared to larger vehicles, making them more susceptible to being influenced by lateral winds [5,7]. The aerodynamic characteristics of small vehicles can lead to significant side forces that affect the driver's ability to maintain control, particularly at higher speeds where the impact of crosswinds is amplified [5,6,8]. The stability of these vehicles can be further compromised by their design, which may not be optimized for handling crosswind forces, increasing the likelihood of skidding or rolling over in extreme conditions [9,10].

Safety hazards associated with crosswinds are particularly pronounced at higher speeds or on open roads where the vehicle is more exposed to gusts of wind. Studies have shown that aerodynamic forces acting on vehicles can lead to a reduction in stability, increasing the risk of accidents [6,11,12]. For instance, vehicles can experience sudden lateral shifts, which may result in a loss of control, especially if the driver is unprepared for the sudden change in handling dynamics [13-15]. This risk is particularly critical for small city vehicles, which may not have the same structural integrity or weight to counteract these forces as larger vehicles [10], a factor contributing to the growing demand for more compact, energy-efficient transportation solutions.

While considerable research has been conducted on vehicle aerodynamics under steady, normal wind conditions, there remains a gap in studies specifically addressing how crosswinds impact the aerodynamic performance of small city vehicles. Small vehicles, due to their compact size and lightweight structure, exhibit unique aerodynamic behavior compared to larger vehicles, particularly under crosswind conditions. Existing aerodynamic models often fail to account for the specific challenges posed by crosswind-induced forces, which can significantly alter vehicle stability, drag, and driver comfort. This gap emphasizes the need for more focused research to explore the effects of crosswinds on small city vehicles, with the goal of developing more accurate and better design solutions. The primary aim of this study is to analyze the aerodynamic performance of small city vehicles under crosswind conditions.

## 2. Methodology

### 2.1 Geometry Modelling

In this study, a full-scale model of a simplified small city vehicle concept was developed, inspired by the Podbike e-bike car, designed by Per Hassel Sørensen. The Podbike is renowned for its compact and efficient design, merging the features of a bicycle and a car to create an innovative urban transport solution [16]. The model was created using SolidWorks 3D modelling software, capturing the key characteristics of the original vehicle. With dimensions of 2.3 meters in length, 0.8 meters in width, and 1.5 meters in height (as shown in Figure 1), the model reflects the vehicle's compact nature and suitability for urban environments. By simplifying the design, the study focuses on the most critical performance aspects while preserving essential geometric and aerodynamic features. This reduction in complexity enables more efficient simulations, conserving both time and computational resources.

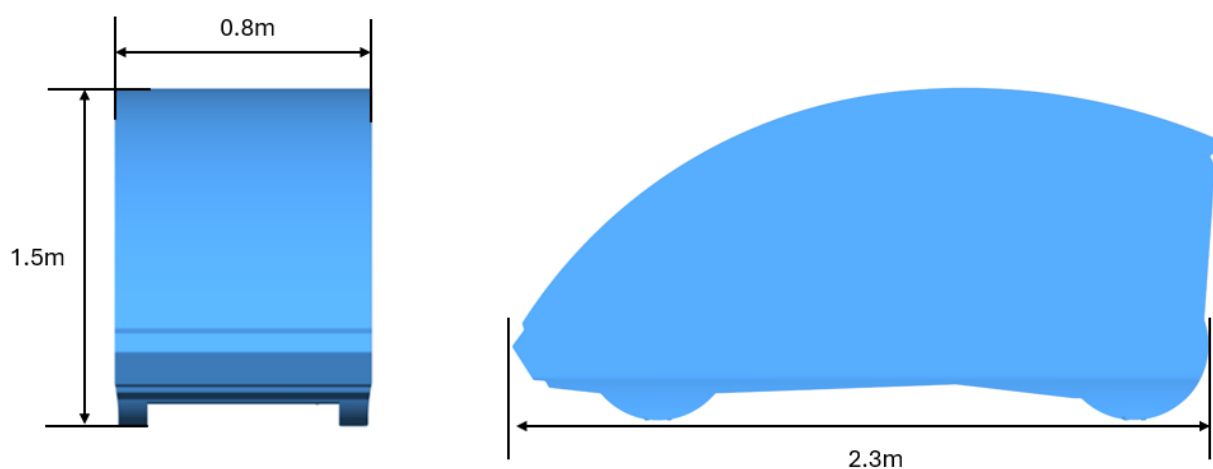
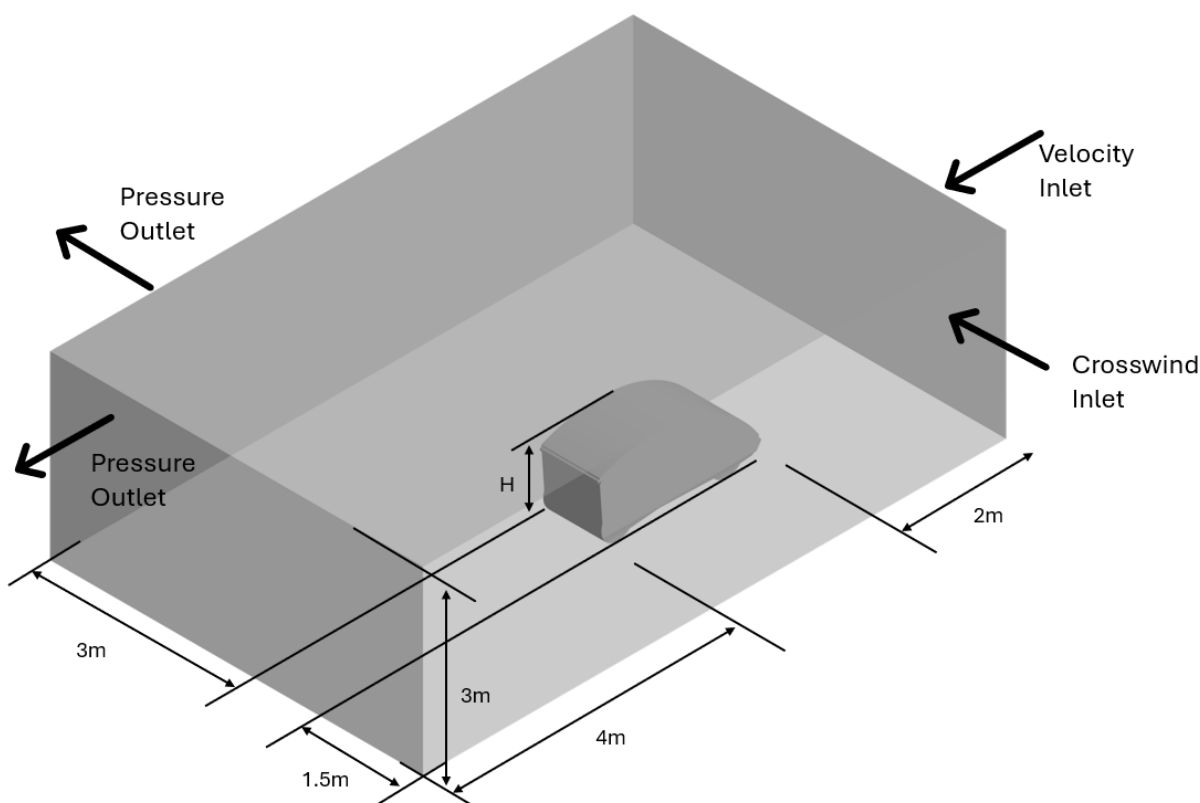


Fig. 1. Dimensions of the simplified small city vehicle designed in SolidWorks

### 2.2 Boundary Conditions and Simulation Setup

The computational domain was defined to include the full-scale vehicle model and be sufficiently large in all directions to reduce the impact of boundary effects on the results [17]. Figure 2 displays the computational domain employed in the current study.

The simulation's boundary conditions were set up to produce accurate and relevant results for small city vehicles scenarios. A constant velocity inlet at 30m/s was applied to the upstream boundary, and the crosswind angle was set to 15°, 30°, 45°, and 60°. A pressure outlet condition at the downstream barrier allowed the flow to escape freely, with atmospheric pressure set to replicate an open environment [18]. The vehicle's surface was modelled as a no-slip wall, assuring zero relative fluid velocity and accurate capture of boundary layer growth and drag forces. The ground plane was also considered as a no-slip wall, with a steady ground condition because the interaction between the vehicle and the road surface is minimal [19]. In addition, the side and roof walls of the domain were considered as symmetry boundary requirements [20].



**Fig. 2.** Computational domain including the dimensions

Reynolds-Averaged Navier-Stokes (RANS) methods were used in this study to accurately portray the effects of turbulence in the flow surrounding the small city vehicles model. The details of the solver settings are shown in Table 1. For the steady-state simulations, the standard k-epsilon model was used with standard wall functions to treat the near-wall region [21]. The SIMPLE algorithm was employed for pressure-velocity coupling, ensuring stable and convergent solutions [22]. Spatial discretization for gradients was performed using the Green-Gauss cell-based method. The SIMPLE algorithm was also used for pressure-velocity coupling.

**Table 1**

The turbulence modelling parameters for Reynolds-Averaged Navier-Stokes (RANS) approach used in the simulations

Parameter	RANS
Model	k-epsilon
Type	Standard
Wall treatment	Standard wall functions
Solver type	Steady
Number of Iterations / Time Steps	1000
Pressure velocity coupling	SIMPLE
Spatial discretization (Gradient)	Green-Gauss cell based
Pressure	Second order
Momentum	Second order upwind
Turbulent kinetic energy	First order upwind
Turbulent dissipation rate	First order upwind

### 2.3 Mesh Independence Study

In the Ansys Advanced meshing module, the computational domain surrounding the vehicle was meshed using a Cartesian grid to break down the geometry into smaller parts. The meshing approach is intended to achieve a balance between resolution and computing efficiency. Mesh independence research was performed to determine the sensitivity of simulation results to mesh resolution modifications. This study involved systematically refining the mesh and examining how drag coefficients converged as mesh refinement increased. Table 2 contains the details of the meshing approach and associated meshing parameters.

**Table 2**  
Meshing parameter descriptions

Parameters	Mesh 1	Mesh 2	Mesh 3
Number of elements	313794	675082	2811807
Total nodes	368874	763202	2946133
Element size (mm)	128	64	32
Face size (mm)	4	2	1
Drag Coefficient, $C_d$	0.568	0.546	0.541

Simulations were run using a coarse mesh with an element size of 128 mm, and the results were analysed. Figure 3 shows how the mesh was improved gradually, reducing the element size consistently across three different resolutions. Surface mesh sizes ranged from 4 mm for the coarsest mesh (Mesh 1) to 1 mm for the finest mesh (Mesh 3), with a total of 2.8 million elements in Mesh 3. Meanwhile, for all cases, the orthogonal mesh quality exceeded 0.75. The drag coefficient results showed consistent changes when the mesh was adjusted. The percentage inaccuracy between Mesh 1 and Mesh 2 was around 4%, demonstrating a significant improvement with finer resolution. Further refining between Mesh 2 and Mesh 3 demonstrated less than 1% inaccuracy.

Based on these findings, Mesh 2 was identified as sufficient for predicting aerodynamic loads, as it provided accurate results with minimal computational expense compared to Mesh 3. This approach ensures that the simulation setup is optimized for efficiency while maintaining reliability in predicting the small city vehicle model's aerodynamic performance. Based on these findings, Mesh 2 was determined to be sufficient for estimating aerodynamic loads because it produced accurate estimations at a lower computational cost than Mesh 3. This approach ensures that the simulation setup is optimized for efficiency while accurately predicting the aerodynamic performance of the small city car model.

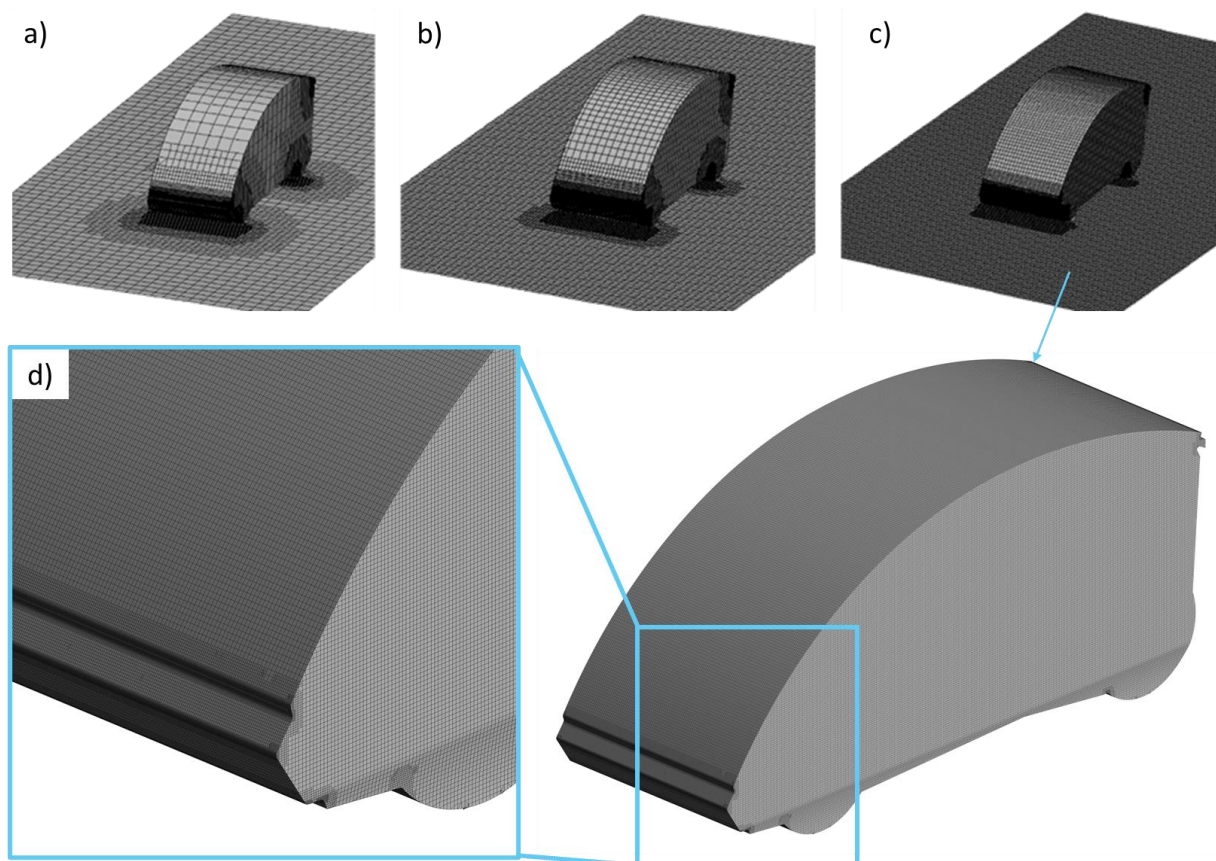


**Fig. 3.** Three different mesh resolutions; (a) mesh 1, (b) mesh 2 and (c) mesh 3, (d) detail mesh

### 3. Results

#### 3.1 Aerodynamic Forces

In this section, we present a detailed comparison of the aerodynamic force coefficients, specifically drag, side, lift and rolling moment values calculated at four different crosswind angles: 15°, 30°, 45°, and 60°. We evaluate these coefficients using the traditional RANS (Reynolds-Averaged Navier-Stokes) model shown in Figure 4. The RANS model used in this study is the  $k-\epsilon$ , which relies on time-averaged Navier-Stokes equations and turbulence closure relationships to predict aerodynamic forces.

At 15°,  $C_d$  is measured at 0.713, indicating moderate drag. With an increase in crosswind angle to 30°,  $C_d$  slightly increases to 0.737, suggesting that this crosswind angle produces slightly higher aerodynamic resistance. However, as the angle increases to 45°,  $C_d$  drops to 0.539, indicating a reduction in drag possibly due to changes in the vehicle's aerodynamic profile as the crosswind redirects airflow around the vehicle differently. Notably, at a 60° crosswind,  $C_d$  becomes negative, measured at -0.007, which could indicate a change in the vehicle's aerodynamic flow that results in an unusual reduction in drag or a slight thrust effect from the crosswind direction.

At a 15° crosswind angle,  $C_s$  is 1.557, indicating moderate lateral force. As the angle rises to 30°,  $C_s$  increases significantly to 2.727, showing that crosswinds create stronger lateral forces that could impact vehicle stability. At 45°,  $C_s$  reaches 3.905, marking a further escalation in side force and emphasizing the vehicle's increased susceptibility to lateral displacement in higher crosswinds. Finally, at 60°,  $C_s$  peaks at 5.017, highlighting that high crosswind angles substantially increase side forces, which could lead to control challenges, especially at higher vehicle speeds or in lightweight vehicles [23].

At a crosswind angle of 15°,  $C_l$  is recorded at 0.307, indicating a small lift effect. When the angle increases to 30°,  $C_l$  nearly doubles to 0.712, suggesting a higher lift due to the crosswind, which could reduce tire contact with the road and compromise stability. As the angle reaches 45°,  $C_l$  increases further to 0.921, signifying a considerable lift effect that could impact vertical stability and handling. However, at 60°,  $C_l$  decreases to 0.626, reflecting a reduction in lift that could enhance stability by lowering the lift effect on the vehicle, potentially improving road grip and control at this extreme angle.

At 15°,  $C_{rm}$  is 0.681, indicating a moderate potential for rolling. As the crosswind angle increases to 30°,  $C_{rm}$  slightly rises to 0.699, showing an incremental increase in the rolling effect due to crosswind. However, at 45°,  $C_{rm}$  decreases to 0.475, suggesting that aerodynamic changes at this angle may reduce the rolling moment, thereby enhancing the vehicle's stability. At 60°,  $C_{rm}$  further decreases to 0.294, indicating a significant reduction in the rolling moment at high crosswind angles, due to flow separation effects around the vehicle, leading to a decrease in lateral rolling forces.

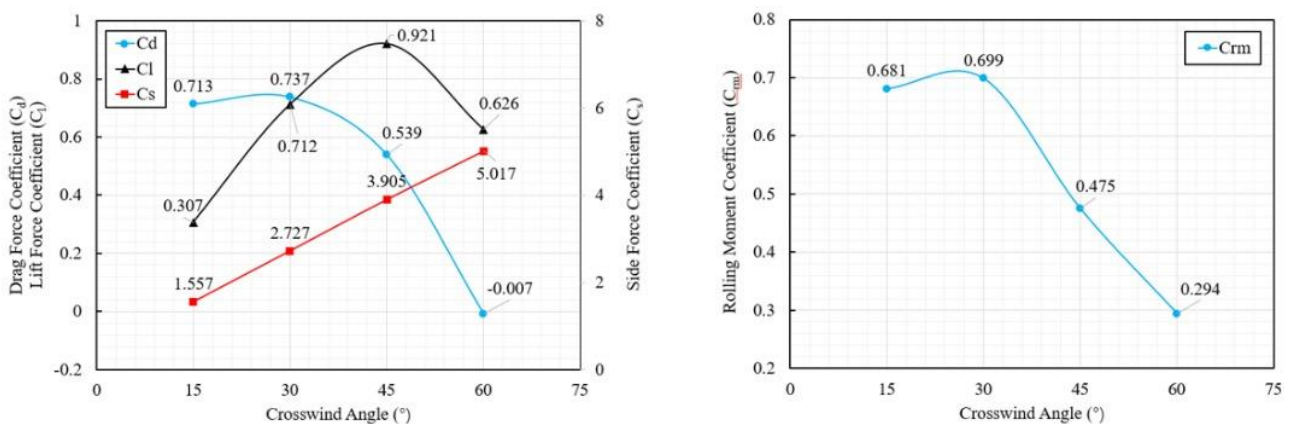


Fig. 4. Drag, side, lift and rolling moment coefficient at different crosswind angles for RANS

### 3.2 Three-Dimensional Vortex Core

Figure 5 shows a series of flow visualizations around the vehicle model for different crosswind angles. At a crosswind angle of 15°, the vortex cores are relatively small and stable. In the rear view, minor vortex structures are visible around the rear edges and lower sections of the vehicle, with velocity concentrated in the lower range. From the front view, the vortex structures are predominantly concentrated around the lower front and sides, indicating that the airflow remains attached to the vehicle body, with minimal disruption. These characteristics imply stable flow behaviour with minimal vortex-induced drag and lift, contributing to improved vehicle stability under mild crosswind conditions. With a 30° crosswind, the vortex core regions around the vehicle become more pronounced and complex. In the rear view, larger vortex structures are observed near the rear and side sections, with a noticeable increase in velocity indicated by the shift to green and yellow colours. These stronger vortex cores suggest greater aerodynamic disturbance as the crosswind angle rises, generating higher drag and lift forces. The front view shows the vortices extending along the side surfaces, with vortex cores developing near the front and roof areas. These vortices reflect increased airflow separation due to the higher crosswind angle, resulting in amplified side forces and potential instability as the vortices create additional aerodynamic load on the vehicle's surfaces.

At 45°, the vortex cores are significantly larger, with high-velocity regions forming around the sides and rear sections in the rear view. This increase in velocity and vortex intensity highlights the amplified aerodynamic interference as the crosswind angle becomes steeper. The vortex cores

extend further away from the vehicle body, indicating intensified flow separation, which contributes to a substantial rise in drag and lift forces. In the front view, the vortex cores appear more prominent, with complex swirling patterns along the sides and top of the vehicle. This substantial vortex development around the front and roof areas demonstrates heightened lateral aerodynamic loads, potentially leading to instability as the crosswind disrupts the airflow, generating turbulent wake zones. At the extreme crosswind angle of 60°, the vortex cores exhibit the most extensive and intense patterns, with substantial high-velocity zones. The rear view reveals large, detached vortex structures that extend significantly behind the vehicle, signifying pronounced flow separation and turbulent wake formation. This dramatic separation of vortex cores from the vehicle body leads to a considerable increase in drag and a potential reduction in aerodynamic stability. From the front, the vortex structures are highly developed along the entire side profile, with complex swirling regions that stretch from the front to the rear. These prominent vortex patterns indicate that the vehicle experiences substantial lateral and lift forces under extreme crosswind conditions, which could lead to significant stability challenges for the driver.

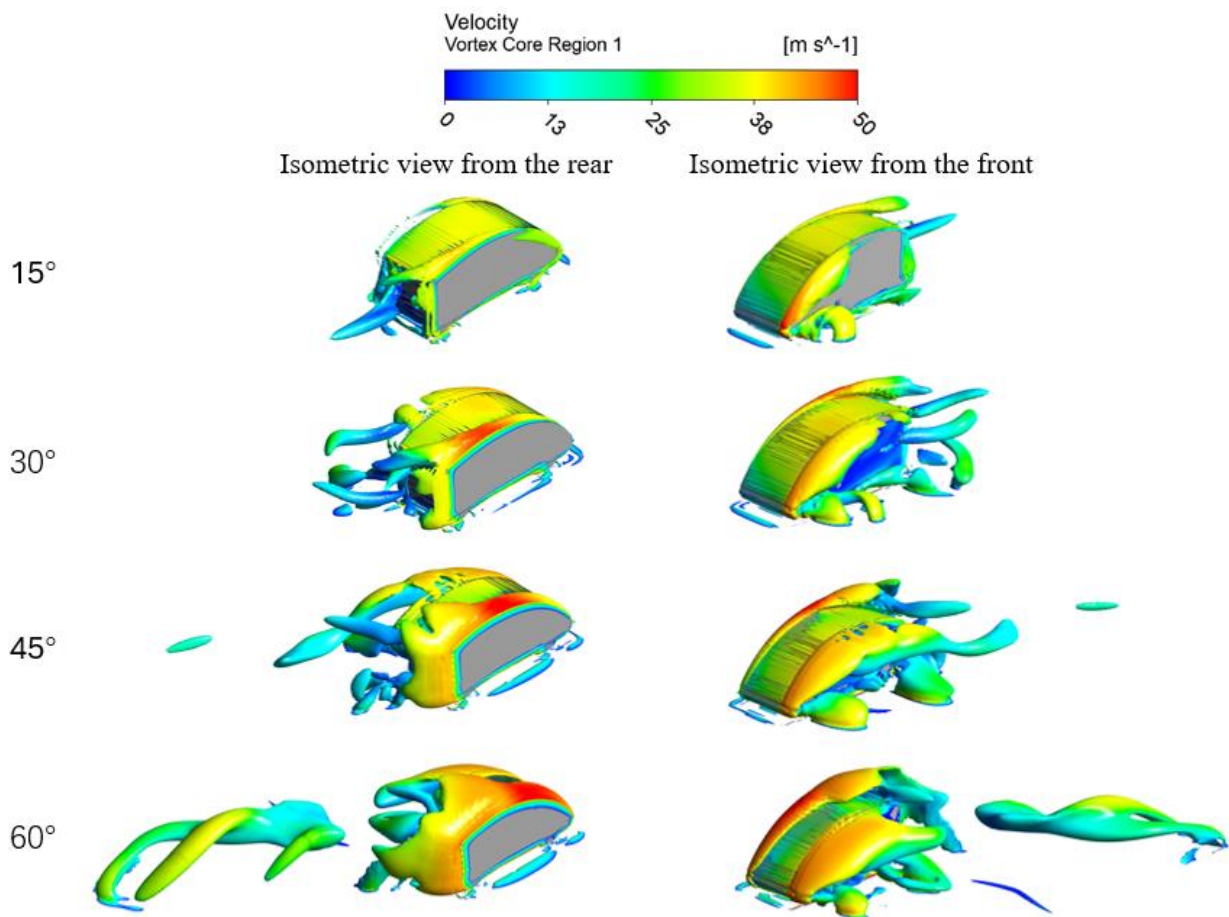


**Fig. 5.** Iso surface of the  $Q$ -criterion coloured with velocity for vehicle

As the crosswind angle increases to 45°, the vortex cores become larger and more intense, especially around the rear and side sections. This intensification reflects greater aerodynamic interference, with more pronounced flow separation and higher lateral forces, which could affect vehicle stability. At the extreme crosswind angle of 60°, the vortex structures are extensive and detached from the vehicle, creating a turbulent wake zone. This detachment results in significant drag and increased lateral and lift forces, potentially compromising control and stability.

### 3.3 Velocity Characteristics around the Vehicle

Figure 6 presents a detailed comparison between different crosswind angles for flow around a simplified vehicle geometry at plane  $y = -0.2$ . It highlights the velocity field in the flow plane and the streamline at three different crosswind angles: 15°, 30°, 45°, and 60°. It illustrates the flow acceleration over the vehicle and deceleration in the wake region. The streamlines in the figure indicate the flow direction and behaviour, providing a clear visualization of the aerodynamic performance under different conditions.

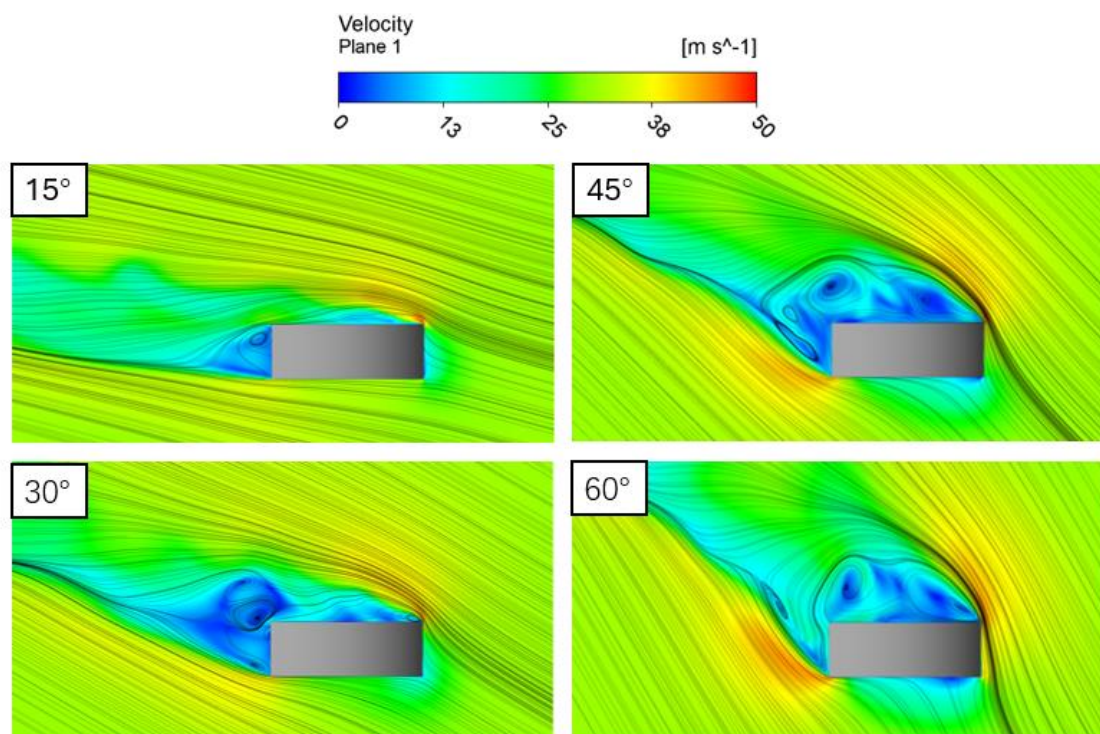


**Fig. 6.** Comparison of the velocity field in the flow plane and streamline on the vehicle surface at four different crosswind angles  $y = -0.2$

At a crosswind angle of 15°, the flow structure around the vehicle remains relatively smooth and attached, with minimal flow separation. The streamlines in the wake region display an orderly pattern, with minor circulation visible near the rear. The low-velocity region is confined close to the vehicle's leeward side, with a gradual transition to higher velocities in the surrounding flow. This relatively stable and low-separation flow pattern indicates that the vehicle experiences minimal aerodynamic disturbance at a 15° crosswind angle, resulting in lower drag and reduced lateral forces, contributing to stable vehicle handling. As the crosswind angle increases to 30°, the flow structure becomes more complex, with the development of larger vortices and an increase in flow separation. The streamlines show notable recirculation near the rear, with more pronounced low-velocity regions on the leeward side, suggesting that the flow is beginning to detach from the vehicle surface. The wake zone behind the vehicle becomes more turbulent, as seen by the swirling streamline patterns, which indicate the formation of vortices. This increased flow separation contributes to higher drag and side forces, potentially impacting the vehicle's aerodynamic stability and making it more susceptible to lateral displacement by crosswinds.

At a 45° crosswind angle, the flow separation becomes even more pronounced, with large, well-defined vortices forming in the wake region. The streamlines reveal a significant increase in

recirculation zones, with low-velocity areas expanding around the leeward side and wake. The intense swirling motion in the wake indicates higher aerodynamic interference, as the airflow detaches more significantly from the vehicle's surface. The high turbulence in the wake zone increases drag and side forces, likely resulting in substantial lateral instability. At this angle, the aerodynamic loads on the vehicle are considerable, making the vehicle more vulnerable to crosswind effects and necessitating better control measures to maintain stability [24]. At the extreme angle of 60°, the flow structure exhibits maximum separation and turbulence, with extensive vortex formation in the wake region. The streamline patterns show large recirculation zones and low-velocity regions that extend far behind and to the side of the vehicle, reflecting substantial flow detachment. The strong swirling vortices indicate intense aerodynamic disturbances, leading to very high drag and lateral forces. This degree of flow separation and turbulence severely impacts vehicle stability, creating substantial aerodynamic loads that make the vehicle difficult to control under extreme crosswind conditions. At this angle, the vehicle's design would need to account for significant lateral and lift forces to counteract the instability caused by the pronounced flow separation. As the crosswind angle increases from 15° to 60°, the flow structure around the vehicle becomes increasingly separated, with larger and more intense vortices forming in the wake region. Lower crosswind angles (15° and 30°) show relatively stable and attached flow patterns, contributing to reduced aerodynamic disturbance. At higher crosswind angles (45° and 60°), the flow separation intensifies, with extensive vortex formation and low-velocity regions, resulting in higher drag, side forces, and lateral instability.

Furthermore, Figure 7 illustrates the surface pressure distribution on a vehicle subjected to different angles, specifically 15°, 30°, 45°, and 60°. Each row represents a different orientation, showing the left and right sides of the vehicle to highlight pressure variations. At a 15° orientation, the pressure distribution is mostly even across the vehicle's surface. On the left side, there is a gradual pressure gradient, with a higher pressure at the front that smoothly decreases toward the rear. This gradual transition suggests that airflow remains stable along the surface without significant disruptions, which would indicate minimal drag forces. On the right side, a similar distribution is observed, showing a consistent decrease in pressure from the front to the rear. The minimal pressure gradient and lack of abrupt changes in pressure imply low drag and stable aerodynamic behaviour, which are desirable for fuel efficiency and vehicle stability. When the angle increases to 30°, the pressure distribution shows a noticeable high-pressure region at the front, highlighted in red and orange. This high-pressure area indicates a stronger aerodynamic impact, which results in increased drag. Moving toward the rear, the pressure gradient becomes steeper, suggesting that airflow may begin to separate from the surface, potentially leading to turbulence. On the right side, the pattern is consistent, with a strong pressure build up at the front and a quick drop toward the rear. The intensified pressure gradient at this angle implies a higher aerodynamic drag compared to the 15° orientation, which can reduce fuel efficiency and slightly impact stability due to turbulent airflow patterns.

At a 45° orientation, the vehicle experiences a more significant aerodynamic impact. The high-pressure region at the front becomes larger and more intense, with the red and orange areas extending further along the surface. This intense pressure distribution at the front causes substantial drag, as the airflow faces greater resistance. The sharp pressure drop toward the rear suggests more extensive flow separation, creating a larger wake region and increasing turbulence. This distribution on the right side also shows a similar trend, with a strong high-pressure zone at the front and an abrupt gradient toward the back. The pronounced flow separation and large wake area at this angle indicate reduced aerodynamic efficiency and a higher likelihood of instability due to turbulent airflow. Finally, at a 60° orientation, the pressure distribution reaches its peak in terms of

aerodynamic impact. The high-pressure region at the front is the most saturated and extensive, covering a larger area than in any other orientation. This suggests that the vehicle experiences maximum drag at this angle. The right side mirrors this pattern, showing a strong high-pressure front and an abrupt drop in pressure as airflow moves toward the rear. This sharp transition indicates severe flow separation and a large wake region, contributing to high aerodynamic drag and increased turbulence. At this orientation, the vehicle's stability and efficiency would be the most compromised due to the intense aerodynamic forces acting on it.

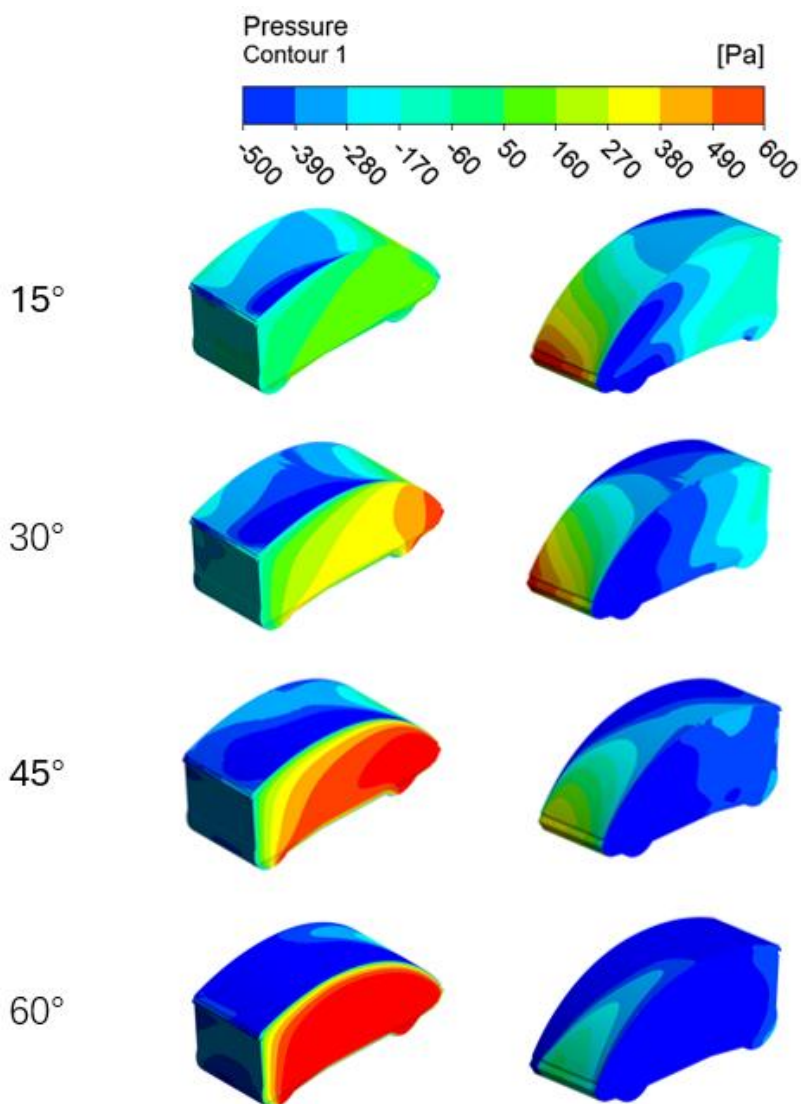


**Fig. 7.** Comparison of surface pressure distribution on vehicle at four different crosswind angles

#### 4. Conclusions

This study evaluated the aerodynamic performance of a simplified small city vehicle under varying crosswind conditions using the Reynolds-Averaged Navier-Stokes (RANS) model.

The results revealed significant variations in aerodynamic forces: drag, side force, lift, and rolling moment at different crosswind angles. As the crosswind angle increased from 15° to 60°, drag forces initially increased before decreasing at higher angles, with the most notable changes occurring in side forces and lift, which escalated under stronger crosswinds. The vortex core analysis further

highlighted the growing intensity of flow separation and turbulence with increasing crosswind angles, contributing to higher drag and lateral instability.

In practical terms, the findings suggest that the vehicle's aerodynamic design is more sensitive to high crosswinds, which can significantly affect its stability and performance, particularly in urban environments. The results emphasize the importance of considering crosswind effects in the design of small city vehicles, where stability and energy efficiency are essential. Future work could explore design modifications aimed at mitigating the aerodynamic challenges posed by crosswinds.

## Acknowledgement

This research was not funded by any grant.

## References

- [1] Eberz, Thomas, and Philip Newnham. "Aerodynamic Development of the Ford Kuga." *ATZ worldwide* 122, no. 9 (2020): 54-60. <https://doi.org/10.1007/s38311-020-0287-9>
- [2] Wu, Jiarong, and Yiding Wen. "Methods on Adjusting Vehicle's Shape to Control Air Resistance." *Highlights in Science, Engineering and Technology* 13 (2022): 14-20. <https://doi.org/10.54097/hset.v13i.1310>
- [3] Nath, Devang S., Prashant Chandra Pujari, Amit Jain, and Vikas Rastogi. "Drag reduction by application of aerodynamic devices in a race car." *Advances in Aerodynamics* 3 (2021): 1-20. <https://doi.org/10.1186/s42774-020-00054-7>
- [4] Tsubokura, Makoto, Takuji Nakashima, Masashi Kitayama, Yuki Ikawa, Deog Hee Doh, and Toshio Kobayashi. "Large eddy simulation on the unsteady aerodynamic response of a road vehicle in transient crosswinds." *International Journal of Heat and Fluid Flow* 31, no. 6 (2010): 1075-1086. <https://doi.org/10.1016/j.ijheatfluidflow.2010.05.008>
- [5] Lim, Wei Chen, Izuan Amin Ishak, Mohammad Arafat, Muhammad Nabil Farhan Kamal, Nor Afzanizam Samiran, and Ahmad Faiz Mohammad. "Analysis of the Aerodynamic Characteristics of Small-Sized Car Vehicles under the Influence of Steady Crosswind." *International Journal of Application on Sciences, Technology and Engineering* 1, no. 1 (2023): 217-224. <https://doi.org/10.24912/ijaste.v1.i1.217-224>
- [6] Huang, Taiming, Zhengqi Gu, Chengjie Feng, and Wei Zeng. "Transient aerodynamics simulations of a road vehicle in the crosswind condition coupled with the vehicle's motion." *Proceedings of the Institution of Mechanical Engineers, Part D: Journal of automobile engineering* 232, no. 5 (2018): 583-598. <https://doi.org/10.1177/0954407017704609>
- [7] Brandt, Adam, Bengt Jacobson, and Simone Sebben. "High speed driving stability of road vehicles under crosswinds: an aerodynamic and vehicle dynamic parametric sensitivity analysis." *Vehicle system dynamics* 60, no. 7 (2022): 2334-2357. <https://doi.org/10.1080/00423114.2021.1903516>
- [8] Huang, T. M., Z. Q. Gu, and C. J. Feng. "Coupled analysis of unsteady aerodynamics and vehicle motion of a passenger car in crosswind condition." *Journal of Applied Fluid Mechanics* 10, no. 2 (2017): 625-637. <https://doi.org/10.18869/acadpub.jafm.73.239.26639>
- [9] Arafat, Mohammad, and Izuan Amin Ishak. "CFD analysis of the flow around simplified next-generation train subjected to crosswinds at low yaw angles." *CFD Letters* 14, no. 3 (2022): 129-139. <https://doi.org/10.37934/cfdl.14.3.129139>
- [10] Rui, Wang, Xu Lei, Shi Feng, Zhang HaoQi, Wang Wenjie, and Lai Xinhe. "Influencing factors of crosswind environment on vehicle running safety and analysis of driving stability." In *International Conference on Smart Transportation and City Engineering (STCE 2023)*, vol. 13018, pp. 62-70. SPIE, 2024. <https://doi.org/10.1117/12.3024037>
- [11] Li, Shuya, Zhengqi Gu, Taiming Huang, Zhen Chen, and Jun Liu. "Coupled analysis of vehicle stability in crosswind on low adhesion road." *International Journal of Numerical Methods for Heat & Fluid Flow* 28, no. 8 (2018): 1956-1972. <https://doi.org/10.1108/HFF-01-2018-0013>
- [12] Paradot, Nicolas, Rémi Grégoire, Marc Stiepel, Ander Blanco, Mikael Sima, Peter Deeg, Kaspar Schroeder-Bodenstein, Terry Johnson, and Gianluca Zanetti. "Crosswind sensitivity assessment of a representative Europe-wide range of conventional vehicles." *Proceedings of the Institution of Mechanical Engineers, Part F: Journal of Rail and Rapid Transit* 229, no. 6 (2015): 594-624. <https://doi.org/10.1177/0954409715585368>
- [13] Jannat, Mafruhatul, and Katharine M. Hunter-Zaworski. "Planning Secondary Road Network for Low-Speed Vehicles in Small or Medium-Sized City with Google Earth." *Transportation research record* 2307, no. 1 (2012): 60-67. <https://doi.org/10.3141/2307-07>
- [14] Tunay, Tural, Lars Drugge, and Ciarán J. O'Reilly. "On coupling methods used to simulate the dynamic characteristics

- of heavy ground vehicles subjected to crosswind." *Journal of Wind Engineering and Industrial Aerodynamics* 201 (2020): 104194. <https://doi.org/10.1016/j.jweia.2020.104194>
- [15] Huang, Taiming, Shuya Li, Zhongmin Wan, and Zhengqi Gu. "Investigation of vehicle stability under crosswind conditions based on coupling methods." *Proceedings of the Institution of Mechanical Engineers, Part D: Journal of automobile engineering* 233, no. 13 (2019): 3305-3317. <https://doi.org/10.1177/0954407018822424>
- [16] Arafat, Mohammad, Izuan Amin Ishak, Muhammad Aidil Safwan Abdul Aziz, Andrew Wee Shong Soh, Woei Ting Tiong, Nur Rasyidah Roziman, Nur Amiza Mohd Hairul et al. "A Hybrid RANS/LES Model for Predicting the Aerodynamics of Small City Vehicles." *Journal of Advanced Research in Experimental Fluid Mechanics and Heat Transfer* 17, no. 1 (2024): 1-13. <https://doi.org/10.37934/arefmht.17.1.113>
- [17] Pirouz, Behrouz, Domenico Mazzeo, Stefania Anna Palermo, Seyed Navid Naghib, Michele Turco, and Patrizia Piro. "CFD investigation of vehicle's ventilation systems and analysis of ACH in typical airplanes, cars, and buses." *Sustainability* 13, no. 12 (2021): 6799. <https://doi.org/10.3390/su13126799>
- [18] Wu, Chengjun, Jiang Liu, and Jie Pan. "Influence of surrounding structures upon the aerodynamic and acoustic performance of the outdoor unit of a split air-conditioner." *Chinese Journal of Mechanical Engineering* 27, no. 4 (2014): 836-845. <https://doi.org/10.3901/CJME.2014.0515.095>
- [19] Abe, Masato. "Vehicle dynamics and control." *Vehicle Handling Dynamics* (2015): 1-3. <https://doi.org/10.1016/B978-0-08-100390-9.00001-4>
- [20] Favre, Tristan, and Gunilla Efraimsson. "An assessment of detached-eddy simulations of unsteady crosswind aerodynamics of road vehicles." *Flow, Turbulence and Combustion* 87 (2011): 133-163. <https://doi.org/10.1007/s10494-011-9333-4>
- [21] Niu, Jiqiang, Yueming Wang, Feng Liu, and Rui Li. "Aerodynamic behavior of a high-speed train with a braking plate mounted in the region of inter-car gap or uniform-car body: A comparative numerical study." *Proceedings of the Institution of Mechanical Engineers, Part F: Journal of Rail and Rapid Transit* 235, no. 7 (2021): 815-826. <https://doi.org/10.1177/0954409720965821>
- [22] Chamkha, Ali J., and Younes Menni. "Hydrogen Flow over a Detached V-Shaped Rib in a Rectangular Channel." *Mathematical Modelling of Engineering Problems* 7, no. 2 (2020). <https://doi.org/10.18280/mmep.070202>
- [23] Kamal, Muhammad Nabil Farhan, Izuan Amin Ishak, Nofrizalidris Darlis, Nurshafinaz Mohd Maruai, Rahim Jamian, Razlin Abd Rashid, NorAfzanizam Samiran, and Nik Normunira Mat Hassan. "Flow Structure Characteristics of the Simplified Compact Car Exposed to Crosswind Effects Using CFD." *Journal of Advanced Research in Applied Sciences and Engineering Technology* 28, no. 1 (2022): 56-66. <https://doi.org/10.37934/araset.28.1.5666>
- [24] Ismail, Muhammad Pirdaus, Izuan Amin Ishak, Nor Afzanizam Samiran, Ahmad Faiz Mohammad, Zuliazura Mohd Salleh, and Nofrizalidris Darlis. "CFD analysis on the effect of vortex generator on sedan car using ansys software." *International Journal of Integrated Engineering* 14, no. 1 (2022): 73-83.